International Journal of Computer Vision and Image Processing
Volume 6 • Issue 1 • January-June 2016

A Contactless Fingerprint Verification Method using a Minutiae Matching Technique

Tahirou Djara, National University of Benin, Cotonou, Benin
Marc Kokou Assogba, National University of Benin, Cotonou, Benin
Antoine Vianou, National University of Benin, Cotonou, Benin

ABSTRACT

Most of matching or verification phases of fingerprint systems use minutiae types and orientation angle to find matched minutiae pairs from the input and template fingerprints. Unfortunately, due to some non-linear distortions, like excessive pressure and fingers twisting during enrollment, this process can cause the minutiae features to be distorted from the original. The authors are then interested in a fingerprint matching method using contactless images for fingerprint verification. After features extraction, they compute Euclidean distances between template minutiae (bifurcation and ending points) and input image minutiae. They compute then after bifurcation ridges orientation angles and ending point orientations. In the decision stage, they analyze the similarity between templates. The proposed algorithm has been tested on a set of 420 fingerprint images. The verification accuracy is found to be acceptable and the experimental results are promising.

KEYWORDS

Contactless Biometrics, Euclidean Distance, Fingerprint, Minimum Orientation Angle Difference, Verification

1. INTRODUCTION

Biometric authentication has received extensive attention over the past decade with increasing demands in automated personal identification as fingerprints are assumed to be unique across individuals, and fingers of the same individual (Pankanti et al., 2002). However, contact based fingerprint systems have some drawbacks due to skin elasticity, inconsistent finger placement, contact pressure, small sensing area, environment conditions and sensor noise. Additionally, problems like contagious diseases spreading make the use of contact based scanners not very safe. We are then interested in a fingerprint matching method using contactless images for fingerprint verification.

Depending on the application context, a biometric system may be called either a verification system or an identification system (Maltoni et al., 2003). A verification system authenticates a person's identity by comparing the captured biometric reference template pre-stored in the system. It conducts one-to-one comparison to confirm whether the claim of identity by the individual is true. An identification system recognizes an individual by searching the entire enrollment template database for a match. It conducts one-to-many comparisons to establish if the individual is present in the database and if so, returns the identifier of the enrollment reference that matched.

DOI: 10.4018/IJCVIP.2016010102

Fingerprint matching techniques can be coarsely classified into three categories, namely minutiae-based matching (Jain et al., 1997; Medina-pérez et al., 2012), image-based matching (A. Qader et al., 2006; Ito et al., 2009; Jain et al., 2000, Sha et al., 2003) and hybrid matching technique (Khalila et al., 2010; Kumar et al., 2012). Minutiae-based matching essentially consists of finding the alignment between the template and the input minutiae feature sets that result in the maximum number of minutiae pairings.

In this paper, we present a contactless fingerprint verification method using a minutiae matching technique, based on the alignment between template images acquired by a contactless system and input images acquired by the same way. Contactless images have been acquired and stored in a database during an enrollment step. The first stage in an Automatic Fingerprint Verification procedure is to extract minutiae from fingerprints. In our contactless fingerprint verification system, we have implemented a minutia extraction algorithm which has been presented in (Djara et al., 2010). The extracted features are ridge bifurcation, ridge ending and ridges orientations. Authors in (Kumar et al., 2012; He et al., 2002; Virk & Maini, 2012) determine orientations using horizontal axis.

Most of the matching or verification of the fingerprint verification systems use minutiae types and orientation angle to find matched minutiae pairs from the input and template fingerprints (Tiko & Kuosmanen, 2003). Thus, accuracy of the verification stage largely depends on the minutiae extraction process. Unfortunately, due to some non-linear distortion, like excessive pressure and twisting of fingers during enrollment, this process can cause the minutiae features to be distorted from the original. Some authors have used the Smallest Minimum Sum of Closest Euclidean Distance of bifurcation points to improve the accuracy of fingerprint verification (Bhowmik et al., 2009).

To overcome those drawbacks, we work on contactless fingerprint images. After features extraction, we compute Euclidean distances between template minutiae and input image minutiae. We compute then after ridges bifurcation orientations and the ridges ending orientations. In the decision stage, we analyze the similarity between templates. Our algorithm has been tested by computing various similarity scores.

In section 2 we present the experimental condition i.e. the contactless enrollment. Feature representation is presented in section 3. Ridge bifurcation and Ridge ending similarity are described in Section 4. Section 5 presents our minutiae matching algorithm. Section 6 contains the similarity score evaluation. Section 7 presents the protocol used for the matching test. Section 8 presents the experimental results and section 9 concludes the paper.

2. CONTACTLESS ENROLLMENT

After the tragic attacks of September 11, 2001, the need for improved and reliable fingerprint recognition technology drastically increased. Despite the known deficiencies and drawbacks of contact-based fingerprinting, this method is still deployed. Although contactless methods are known for producing distortion free fingerprints, this is a rather new technological development, and very few universities are involved in their development. Among authors interested by contactless fingerprint development, we have (Parziale et al., 2006; Hiew et al., 2007; Mil'shtein et al., 2008). Other authors present in an academic work, recent applications in contactless fingerprint (Milshtein et al., 2011).

2.1. Acquisition Protocol

We have developed a Contactless Biometric Fingerprint Software (CBFS) for the acquisition and processing of our images. The contactless fingerprint acquisition system we present consists of this CBFS to visualize the sharpness of the finger before capture, a webcam for taking digital photo, and

lighting equipment. The user is asked to put his finger in a fixed position, the reverse of his finger on the indicated place and his palm faces the camera. We use a medium-resolution webcam (Logitech Pro9000), driven by an interface as shown in Figure 1. In order to limit travel, a rectangular area is defined on the interface of the camera which will contain the finger before capture. The acquired images are PNG format and have a size of 640x640 . Figure 1-(a) shows the system and Figure 1-(b) shows a screenshot of the user's interface.

The distance between the camera and the finger, and the resolution of the output image are two important parameters in contactless image acquisition. In fact, many distances have been tested, and we find the optimum one is 8cm between the camera and the finger. In our experiment, the camera ensures a resolution of 360 dpi.

Figure 3 shows in (a) and (b) two fingerprints images acquired by a contact of sensor, while Figure 2 shows in (a) and (b) two images obtained using our camera. We notice that, a paramount advantage of contactless image acquisition is that a large image area can be captured quickly compared touch based systems.

Figure 1. Contactless fingerprint acquisition system and Screenshot of CBFS

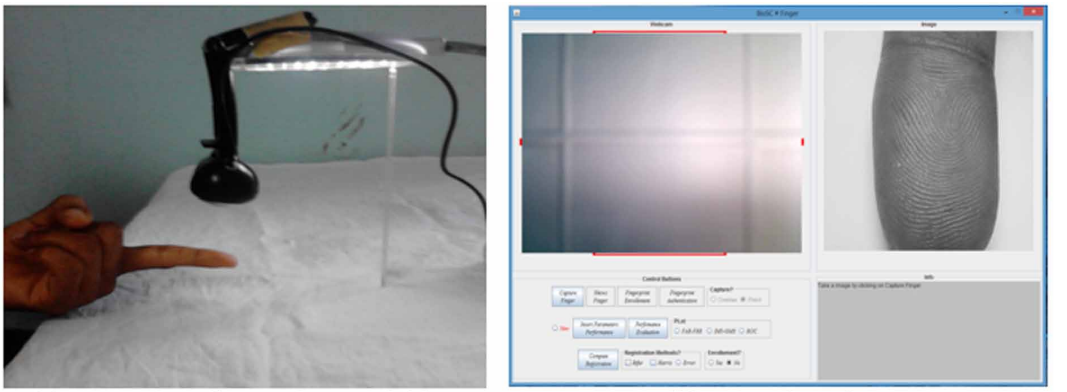

(a) Contactless fingerprint acquisition system

(b) User's interface

Figure 2. Two different acquisitions of the same finger obtained by our webcam

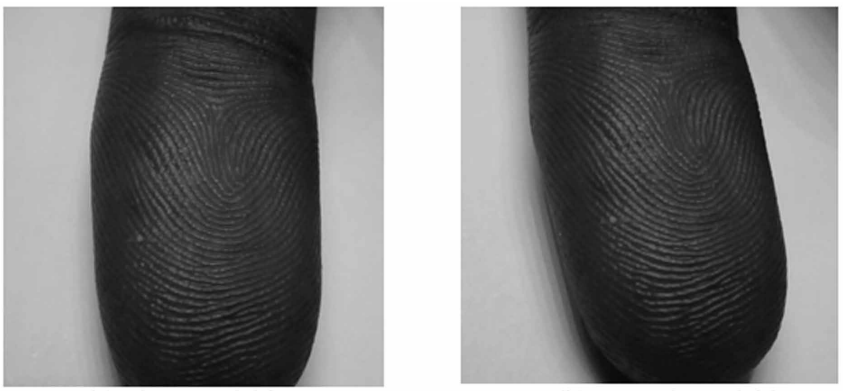

(a) First acquisition

(b) Second acquisition

Figure 3. Two different acquisitions of the same finger obtained by contact-based system (FVC2004 DB1)

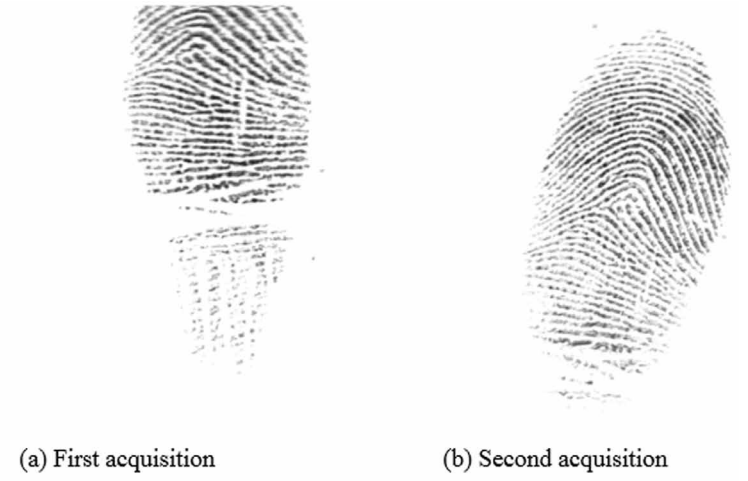

2.2. Pre-Processing Phase

Pre-processing plays a significant role in improving image contrast. We have used histogram equalization for image enhancement. Figure 4.a shows a contactless acquisition fingerprint image while Figure 4.b shows the enhanced image of Figure 4.a. Figure 4.c and 4.d show respectively the histogram of Figure 4.a and Figure 4.b. Images from webcam experiments are Red-Green-Blue color images. The image is converted to grey scale image using the CBFS.

Figure 4. Images and histograms

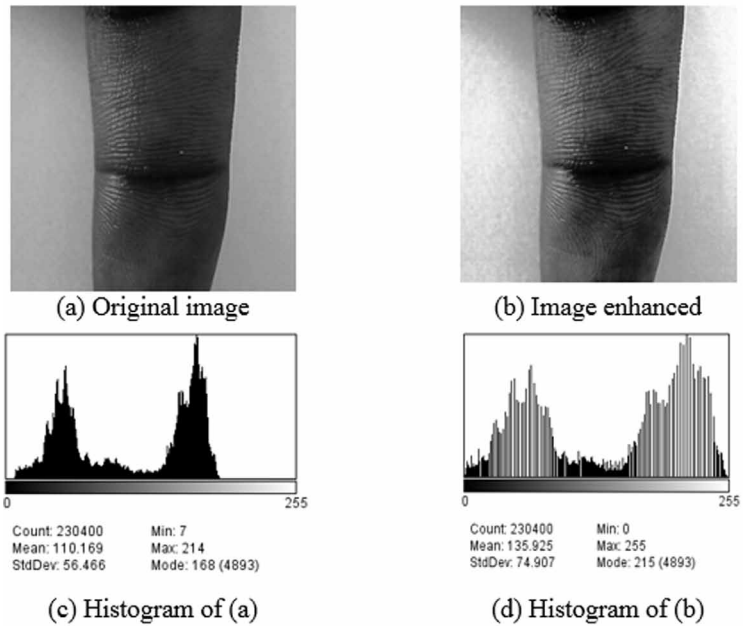

3. FEATURE CHARACTERISATION

The used features are bifurcation points and ending points (Figures 6 and 7). In order to get the streaks in the image of fingerprint, a photometric adaptive threshold method has been developed and presented in (Djara et al., 2010). Two thresholds are defined i.e. S_s and S_h corresponding to the mean of a square framework and the mean of a hexagonal framework. A pixel P is deleted or not by comparing its value with S_s and S_h. Here we introduce the foreground regions extraction before streaks extraction. The extraction phase of the streaks is linked to the extraction foreground regions. For this purpose, we have applied a filter to the image in order to define its contour. Then a binary mask is subsequently applied to the image filter, which allows to have an image defining the contour of the fingerprint. This contour image is used for the extraction of foreground regions (see Figure 5).

The image from the photometric adaptive threshold is skeletonized in order to get minutiae (bifurcation points and ending points). The minutiae are extracted by scanning the local neighborhood of each ridge pixel in the image using a 3×3 window of Table 1. The crossing number (CN) is then

Figure 5. Main steps of the extraction of the foreground regions

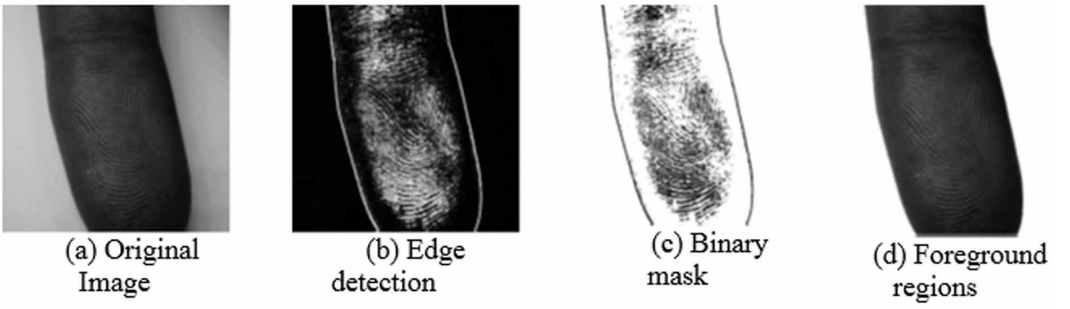

Figure 6. Orientations of bifurcation points

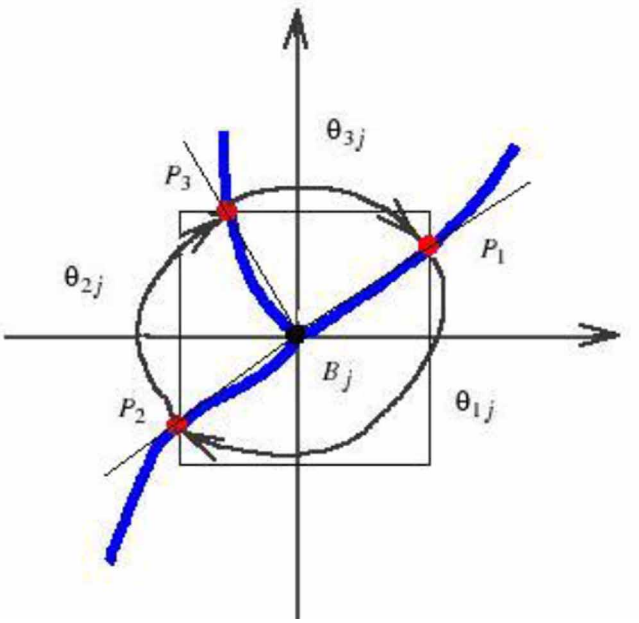

Figure 7. Orientation of ridge ending points

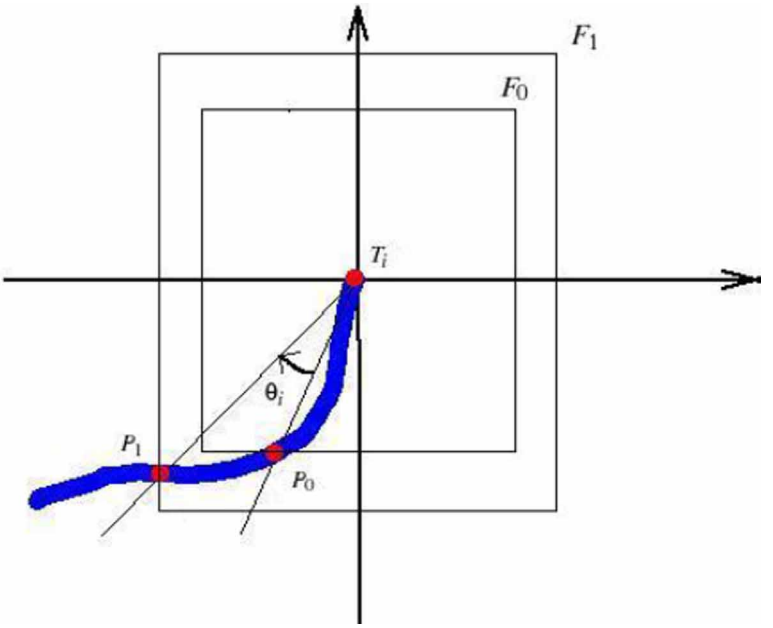

Table 1. 3×3 **operation window**

P_1	P_2	P_3
P_8	P	P_4
P_7	P_6	P_5

computed, which is defined as half the sum of the differences between pairs of adjacent pixels in the eight-neighborhood as presented in (Arcelli & Baja, 1984; Mehtre, 1993). We have:

$$CN = \frac{1}{2}\sum_{i=1}^{8}\left|P_i - P_{i-1}\right|, \quad P_8 = P_0 \tag{1}$$

If $CN = 1$ then the ridge pixel is a ridge ending, while if $CN = 3$ the ridge pixel is a ridge bifurcation otherwise it is a non-minutiae point.

3.1. Ridge Bifurcation Orientation Characterization

In our approach, for bifurcation points we define a window W of size S*S and of central pixel the minutiae points. We count 3 points P_1, P_2, and P_3 around the perimeter of the window as shown in Figure 2.

For a given bifurcation point B_j, we compute the orientations as being (Equations 2, 3 and 4):

$$\theta_{1j} = Arccos\left(\frac{\overrightarrow{B_jP_1}.\overrightarrow{B_jP_2}}{B_jP_1 \times B_jP_2}\right) \tag{2}$$

$$\theta_{2j} = Arccos\left(\frac{\overrightarrow{B_jP_2}.\overrightarrow{B_jP_3}}{B_jP_2 \times B_jP_3}\right) \tag{3}$$

$$\theta_{3j} = Arccos\left(\frac{\overrightarrow{B_jP_3}.\overrightarrow{B_jP_1}}{B_jP_3 \times B_jP_1}\right) \tag{4}$$

(.) stands for the scalar product.
(X) stands for the ordinary multiplication.

For an image with M validated bifurcation points, we build a matrix of M rows and 5 columns. Each point is represented by a row in the matrix. The columns represent the coordinates and the angles between them are the branches.

$$\begin{pmatrix} x_1 & y_1 & \theta_{11} & \theta_{21} & \theta_{31} \\ \cdots & \cdots & \cdots & \cdots & \cdots \\ x_M & y_M & \theta_{1M} & \theta_{2M} & \theta_{3M} \end{pmatrix} \tag{5}$$

3.2. Ridge Ending Orientation Characterization

We define two concentric windows W_1F_0 and W_2F_1 of central point the ridge ending point and for size S_1 and S_2. On the perimeter of F_1W_1 we have a point P_1 and on the perimeter of W_2F_0 we have a point P_2P_0 as shown on Figure 3. For a given ending point T_i, the orientation is defined as the angle between vectors.

$$\theta_{1j} = \mathrm{Arccos}\left(\frac{\overrightarrow{B_jP_1}.\overrightarrow{B_jP_2}}{B_jP_1 \times B_jP_2}\right) \tag{5}$$

$$\theta_i = \mathrm{Arccos}\left(\frac{\overrightarrow{T_iP_0}.\overrightarrow{T_iP_1}}{T_iP_0 \times T_iP_1}\right) \tag{6}$$

(.) stands for the scalar product.
(X) stands for the ordinary multiplication.

For an image with N validated ending points, we build a matrix of N rows and 3 columns. Each row of the matrix represents an ending points. The columns represent the coordinates of the point and the angle of the branch.

$$\begin{pmatrix} x_1 & y_1 & \theta_1 \\ \cdots & \cdots & \cdots \\ x_N & y_N & \theta_{1N} \end{pmatrix} \tag{7}$$

4. RIDGE BIFURCATION AND RIDGE ENDING SIMILARITY

In this section, we introduce the ridge bifurcation (Rb) and the ridge ending points (Re) similarity (Rb-Re Similarity). Let $I_t\left(Rb\right)$ and $I_{t+d}\left(Rb\right)$ be the template and query fingerprint Rb sets respectively. Let $I_t\left(Re\right)$ and $I_{t+d}\left(Re\right)$ be the template and query fingerprint Re sets respectively. We have:

$$I_t\left(b\right)=\left\{b_1,b_2,\ldots,b_M\right\} \qquad b_j=\left(\mathrm{x_j},\mathrm{y_j},\theta_{1j},\theta_{2j},\theta_{3j}\right);\ \ \mathrm{j}\in\left[1\ldots\mathrm{M}\right] \tag{8}$$

$$I_{t+d}\left(b\right)=\left\{b'_1,b'_2,\ldots,b'_{M'}\right\} \qquad b'_P=\left(\mathrm{x'_p},\mathrm{y'_p},\theta'_{1p},\theta'_{2p},\theta'_{3p}\right);\ \ \mathrm{p}\in\left[1\ldots\mathrm{M'}\right] \tag{9}$$

$$I_t\left(t\right)=\left\{t_1,t_2,\ldots,t_N\right\} \qquad t_i=\left(\mathrm{x_i},\mathrm{y_i},\theta_i\right);\ \ \mathrm{i}\in\left[1\ldots\mathrm{N}\right] \tag{10}$$

$$I_{t+d}\left(t\right)=\left\{t'_1,t'_2,\ldots,t'_{N'}\right\} \qquad t'_q=\left(\mathrm{x'_q},\mathrm{y'_q},\theta'_q\right);\ \ \mathrm{q}\in\left[1\ldots\mathrm{N'}\right] \tag{11}$$

where b_j and b'_p represent respectively the $\mathrm{j^{th}}$ and the $\mathrm{p^{th}}$ row of matrix of the Rb. t_i and t'_q represent respectively the $\mathrm{i^{th}}$ and $\mathrm{q^{th}}$ row of matrix of the Re. It is assumed, that there is correspondence between b_j and b'_q if the Euclidean distance (ed) between them is smaller than a given tolerance d_0 and orientation differences (od) of their respective angles are smaller than angular tolerances $\theta_0,\alpha_0,\beta_0$:

$$ed\left(b_j,b'_p\right)=\sqrt{\left(x_j-x'_p\right)^2+\left(y_j-y'_p\right)^2}\le d_0 \tag{12}$$

and

$$\begin{cases} od\left(b_j,b'_p\right)_1=\min\left(\left|\theta_{1j}-\theta'_{1j}\right|,360-\left|\theta_{1j}-\theta'_{1j}\right|\right)\le\theta_0 \\ \qquad\qquad and \\ \begin{cases} od\left(b_j,b'_p\right)_2=\min\left(\left|\theta_{2j}-\theta'_{2j}\right|,360-\left|\theta_{2j}-\theta'_{2j}\right|\right)\le a_0 \\ \qquad\qquad or \\ od\left(b_j,b'_p\right)_3=\min\left(\left|\theta_{3j}-\theta'_{3j}\right|,360-\left|\theta_{3j}-\theta'_{3j}\right|\right)\le\beta_0 \end{cases} \end{cases} \tag{13}$$

By the same way, we assume that there is a correspondence between t_i and t'_q if the euclidean distance (ed) between them is smaller than a given tolerance d_0 and the orientation difference (od) between them is smaller than an angular tolerance θ_0 .

$$ed\left(t_i, t'_q\right) = \sqrt{\left(x_i - x'_q\right)^2 + \left(y_i - y'_q\right)^2} \leq d_0 \tag{14}$$

and

$$od\left(t_i, t'_q\right) = min\left(\left|\theta_i - \theta'_q\right|, 360 - \left|\theta_i - \theta'_q\right|\right) \leq \theta_0 \tag{15}$$

5. MINUTIAE MATCHING

The nature of the deformation between our images is a rigid transformation expressed by:

$$\begin{pmatrix} x' \\ y' \\ 1 \end{pmatrix} = \begin{pmatrix} u_0 & u_1 & u_2 \\ v_0 & v_1 & v_2 \\ 0 & 0 & 1 \end{pmatrix} \begin{pmatrix} x \\ y \\ 1 \end{pmatrix} \tag{16}$$

with

$$\begin{array}{llll} u_0 = \cos(\theta) & u_1 = -\sin(\theta) & u_2 = \left(1 - \cos(\theta)\right) x_0 + y_0 \sin(\theta) + t_x \cos(\theta) - t_y \sin(\theta) \\ v_0 = \sin(\theta) & v_1 = \cos(\theta) & v_2 = \left(1 - \cos(\theta)\right) x_0 + y_0 \sin(\theta) + t_x \sin(\theta) + t_y \cos(\theta) \end{array} \tag{17}$$

where $M_0 \begin{pmatrix} x_0 \\ y_0 \end{pmatrix}$ is the center of rotation, θ the angle of rotation, $\begin{pmatrix} t_x \\ t_y \end{pmatrix}$ the coordinates of the translation vector and $M' \begin{pmatrix} x' \\ y' \end{pmatrix}$, the transform of $M \begin{pmatrix} x \\ y \end{pmatrix}$.

In the research phase of the best deformation, the correspondence between the sets of control points, is obtained by calculating the descriptor vector of Zernike moments on a window of size $L \times L$ centered at each point, taking into account ridges bifurcations. Comparison of correlation coefficients between the descriptors vectors of Zernike moments helps define the corresponding points. The estimation of parameters of the existing deformation between the images is performed using RANSAC algorithm (Random SAmple Consensus) that suppresses wrong matches. The correspondence between these two sets of control points is obtained by following these steps:

- Subdivide each image into thumbnail size $L \times L$ centered on each point B_i .
- For each thumbnail centered on this point B_i , construct the descriptor vector of Zernike moments M_z as follows:

$$M_z = \left(\left|z_{11}\right|,\ldots,\left|z_{pq}\right|,\ldots,\left|z_{55}\right|\right) \tag{18}$$

where $\left|z_{pq}\right|$ is the module of Zernike moments. We have used as the highest order of moments 5 after several experimental trials. Although the higher order moments are the fine details of the image, they are more sensitive to noise than lower order moments. The Zernike moment of order p with repetition q for a continuous image function $f\left(x,y\right)$, that vanishes outside the unit disk is:

$$Z_{pq} = \frac{p+1}{\pi} \iint\limits_{x^2+y^2\le 1} V_{pq}^{*}\left(\rho,\theta\right) f\left(x,y\right) dxdy \tag{19}$$

If F is the digital image of f, the above equation becomes:

$$Z_{pq} = \frac{p+1}{\pi} \sum_{x=1}^{N}\sum_{y=1}^{N} V_{pq}^{*}\left(\rho,\theta\right) F\left(x,y\right) \tag{20}$$

with

$$V_{pq}\left(\rho,\theta\right) = R_{pq}\left(\rho\right) e^{iq\theta} \tag{21}$$

Where R_{pq} is the Zernike radial polynomials of order p with repetition q in $\left(\rho,\theta\right)$ polar coordinates given by:

$$R_{pq}\left(\rho\right) = \sum_{s=0}^{\frac{p-\left|q\right|}{2}} \frac{\left(-1\right)^{s}\left(p-s\right)!}{s!\left(\frac{p+\left|q\right|}{2}-s\right)!\left(\frac{p-\left|q\right|}{2}-s\right)!} \rho^{p-2s} \tag{22}$$

In the above equation p is a non-negative integer, $\left(p \ge 0\right)$, and q positive and negative integers subject to the constraints:

$$\begin{cases} p-\left|q\right| \ is \ even \\ \left|q\right| \le p \end{cases} \tag{23}$$

where V_{pq}^{*} denote complex conjugate of V_{pq}, $\rho = \sqrt{x^2+y^2} \le 1$ and $\theta = tan^{-1}\left(\frac{y}{x}\right)$.

- For any point r_i of the reference image, we suppose that its corresponding e_i of input image is from a set of points located within a certain radius R_0 around r_i. The radius R_0 limits the search

for corresponding and therefore, dramatically reduces the number of comparisons to achieve in order to find out the corresponding points (Figure 8).

- The matching process is performed by calculating the correlation coefficients between the two descriptor vectors. The corresponding points are those which give the maximum value of correlation coefficients.

The correlation coefficient between two vectors of the features $X\left(x_1,\ldots,x_n\right)$ and $Y\left(y_1,\ldots,y_n\right)$ is given by the following formula:

$$C = \frac{\sum_{i=1}^{n}\left(x_i-\overline{x}\right)\left(y_i-\overline{y}\right)}{\sqrt{\sum_{i=1}^{n}\left(x_i-\overline{x}\right)^2}\times\sqrt{\sum_{i=1}^{n}\left(y_i-\overline{y}\right)^2}} \tag{24}$$

where $\overline{x}$ and $\overline{y}$ are averages of the two vectors X and Y respectively. If C is 0, the two vectors are not correlated. The two vectors are better correlated when C is far from 0 (near -1 or 1).

Once the sets of points $I_t\left(.\right)$ and $I_{t+d}\left(.\right)$ are aligned by applying the model of deformation given by Equation 16, the algorithm "Rb-Re Similarity" starts. The formal algorithm is the following (see Figure 9):

The purpose of a match algorithm is to evaluate the similarity of two fingerprints, and to judge whether they belong to the same finger or not. In our method, the similarity value is computed using the formula presented by Galy (2005):

Figure 8. Determining the corresponding e_i (of input image) of a point r_i (of the reference image)

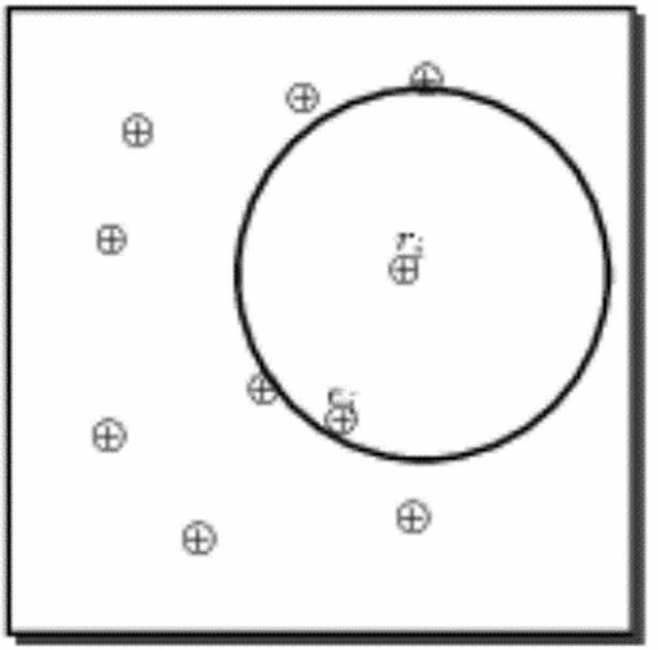

Figure 9. Rb-Re Similarity

```
Let n0 be the maximum number of matching minutiae computed after performing all fingerprint rigid transformation.
Let n1 be the maximum number of matching Rb computed after performing all fingerprint rigid transformation.
Let n2 be the maximum number of matching Re computed after performing all fingerprint rigid transformation.
for i ← 1, M do
    for j ← 1, M′ do
        if RbSimilarity(bi, b′j) then
            n1 ← n1 + 1.
            break.
        end if
    end for
end for
for i ← 1, N do
    for j ← 1, N′ do
        if ReSimilarity(ti, t′j) then
            n2 ← n2 + 1.
            break.
        end if
    end for
end for
n0 ← n1 + n2.
function RbSimilarity(a, b)
    if ed(a,b) ≤ d0 && ( od(a,b)1 ≤ θ0 && ( od(a,b)2 ≤ α0 || od(a,b)3 ≤ β0) ) then
        return true
    else
        return false
    end if
end function
function ReSimilarity(a, b)
    if ed(a,b) ≤ d0 && od(a,b) ≤ θ0 then
        return true
    else
        return false
    end if
end function
```

$$MS = \frac{N}{\max\left(N_{I_t}, N_{I_{t+d}}\right)} \tag{25}$$

where N_{I_t} and $N_{I_{t+d}}$ are the template and query fingerprint minutiae sets respectively, and N is the amount of matching minutiae pairs.

We created a database (available in http://refod.net/images/Fingerprint/DB2.zip) containing 420 prints with 28 different sets of fingers, each with 15 acquisitions.

Let F_{ij} be the j^{th} fingerprint sample of the i^{th} finger and T_{ij} the corresponding template $\left(1 \le i \le n; 1 \le j \le m\right)$. The template T_{ij} are computed from the corresponding F_{ij} and stored on a disk by our platform

For matching, we perform the following operations:

1. **Genuine Matching (GM):** Each fingerprint template T_{ij} is matched against the fingerprint images $F_{ik}\left(k \neq j\right)$ and the corresponding Genuine Matching Score gms_{ijk} are stored.
2. **Impostor Matching (IM):** Each fingerprint template T_{k1} is matched against the fingerprint images from different fingers F_{ij} (i > k) and the corresponding Impostor Matching Score ims_{ik} are stored.

The number of matching is defined in each case:

Case 1: $NGRA = \left\| \left\{ gms_{ijk}, i \in \left[1 \ldots n\right], 1 \leq j \neq k \leq m \right\} \right\| = n * m * \left(m-1\right).$

In our case NGRA = 5880. NGRA is the Number of Genuine Recognition Attempts.

Case 2: $NIRA = \left\| \left\{ ims_{ik}, i \in \left[1 \ldots n\right], 1 \leq j \neq k \leq m \right\} \right\| = m\left[\left(n-1\right) + \left(n-2\right) + \ldots + 1\right].$

In our case NIRA = 5670. NIRA is the Number of Imposter Recognition Attempts.

The GM distribution and the IM distribution are computed and graphically reported to show how the algorithm differentiates the classes. The FMR (False Match Rate) and FNMR (False Non-Match Rate) curves are computed from the above distributions for the threshold t ranking from 0 to 1.

The pairs (FMR(t), FNMR(t)) are plotted for the same value of t to obtained a ROC (Receiver Operating Characteristics) curve.

FMR(t) and FNMR(t) are defined by:

$$FMR\left(t\right) = \frac{card\left\{ ims_{ik} \;/\; ims_{ik} \geq t \right\}}{NIRA} \tag{26}$$

$$FNMR\left(t\right) = \frac{card\left\{ gms_{ik} \;/\; gms_{ijk} < t \right\}}{NGRA} \tag{27}$$

card denote the cardinality of a given set, FMR(t) denotes the percentage of $ims_{ik} \geq t$ and FNMR(t) denotes the percentage of $gms_{ijk} < t$.

6. EXPERIMENTAL RESULTS

Figure 10, shows in (a) GM and IM distributions. In (b) and (c) FMR-FNMR curves and ROC are respectively represented. We evaluate the algorithm performance by using Equal Error Rate (EER) where FMR = FNMR. We notice from Figure 10-(b) that FMR and FNMR values are respectively 7.64% and 6.46% at a threshold (**th**) value of 0.33.

From the database, we achieved an EER to the order of 7.05%. The matching time is approximately 0.6s. The performance of our algorithm is acceptable. The results can be improved ensuring that the database does not contain such poor quality fingerprint images.

Figure 10. GM-IM, FMR-FNMR curves and ROC

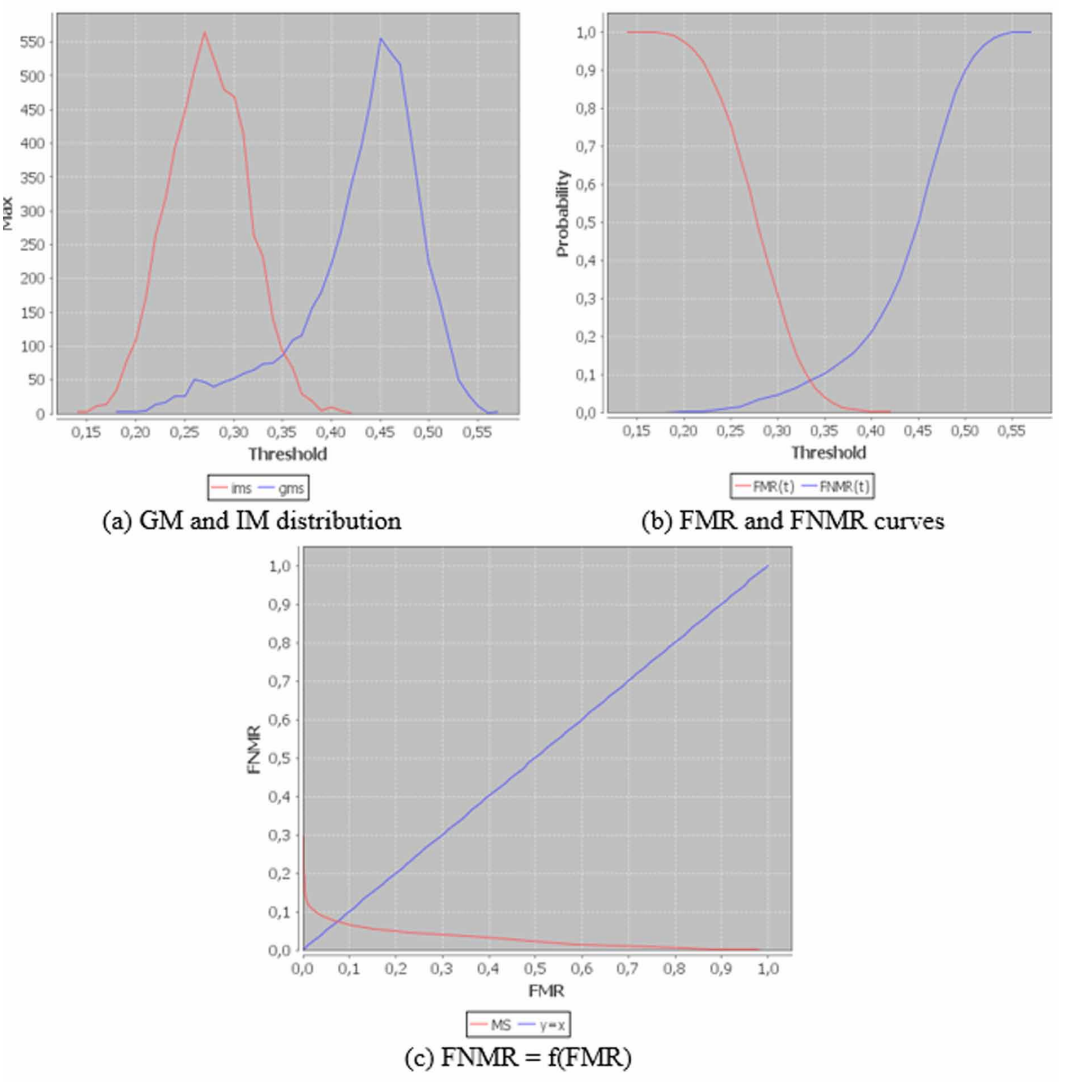

7. CONCLUSION

In this paper, we investigated a fingerprint matching algorithm with only minutiae information as an approach for a supervised contactless biometric system. In this new context, our experiments show that fingerprint images can be well matched using the minutiae matching method. The performance of the algorithms are evaluated through a created database using the CBFS. As shown, we have led 5880 comparisons intra-class (Number of Genuine Recognition Attempts) and 5670 comparisons inter-class (Number of Imposter Recognition Attempts). The illustration of the results available in the contact context shows that the performance of our algorithms are acceptable. The results are encouraging with an Equal Error Rate around 7.05%. In a future work, the performance of our algorithms can be improved by taking into account the 3D fingerprint identification presented in (Ajay & Kwong, 2015; Hong Kong Polytechnic, 2013; Wang et al., 2010).

REFERENCES

Arcelli, C., & Baja, G. S. D. (1984). A width independent fast thinning algorithm. The Institute of Electrical and Electronics Engineers. *Transactions on Pattern Analysis and Machine Intelligence.*, *4*(7), 463–474.

Bhowmik, U. K., Ashrafi, A., & Adhami, R. R. (2009, February). A Fingerprint Verification Algorithm Using the Smallest Minimum Sum of Closest Euclidean Distance. *Proceedings of the International Conference on Electrical, Communications, and Computers CONIELECOMP '09* (pp. 90-95). IEEE. doi:10.1109/CONIELECOMP.2009.57

Djara, T., Assogba, M. K., & Nait-Ali, A. (2010). Caractérisation spatiale des empreintes de l'index en analyse biométrique.*Actes du CARI 2010.* Yamoussoukro (pp. 501-508).

Galy, N. (2005). Etude d'un système complet de reconnaissance d'empreintes digitales pour un capteur microsystème à balayage [Thèse]. Institut National Polytechnique de Grenoble - INPG.

He, Y., Tian, J., Luo, X., & Zhang, T. (2002). Image enhancement and minutiae matching in fingerprint verification. *Pattern Recognition Letters*, 24(9), 1349–1360.

Hiew, B., Teoh, A., & Pang, Y. (2007). Touch-less fingerprint recognition system. Proceedings of*ICB, LNCS* (Vol. *3832*, pp. 24–29).

Ito, K., Morita, A., Aoki, T., Higuchi, T., Nakajima, H., & Kobayashi, K. (2005, September). A fingerprint recognition algorithm using phase-based image matching for low-quality fingerprints. Proceedings of the IEEE International Conference on Image Processing '05 (Vol. 2, pp. II-33). IEEE.

Jain, A., Lin Hong, , & Bolle, R. (1997). al, On-line fingerprint verification. *IEEE Transactions on Pattern Analysis and Machine Intelligence*, *19*(4), 302–314. doi:10.1109/34.587996

Jain, A., Prabhakar, S., Hong, L., & Pankanti, S. (2000). Filterbank-based fingerprint matching. *IEEE Transactions on Image Processing*, *9*(5), 846–859. doi:10.1109/83.841531 PMID:18255456

Khalila, M. S., Mohamada, D., Khanb, M. K., & Al-Nuzailia, Q. (2010). Fingerprint verification using statistical descriptors. *Digital Signal Processing*, *20*(4), 1264–1273. doi:10.1016/j.dsp.2009.12.002

Kumar, A., & Kwong, C. (2015, March). Towards contactless, low-cost, and accurate 3D fingerprint identification. *IEEE Transactions on Pattern Analysis and Machine Intelligence*, *37*(3), 681–696. doi:10.1109/TPAMI.2014.2339818 PMID:26353269

Kumar, R., Chandra, P., & Hanmandlu, M. (2012). Statistical descriptors for fingerprint matching. *International Journal of Computers and Applications*, *59*(16), 24–27. doi:10.5120/9633-4361

Maltoni, D., Maio, D., Jai, A. K., & Prabhakar, A. (2003). *Handbook of fingerprint recognition* (2nd ed., pp. 3–7). New York: Springer.

Medina-Pérez, M. A., García-Borroto, M., Gutierrez-Rodríguez, A. E., & Altamirano-Robles, L. (2012). Improving fingerprint verification using minutiae triplets. Sensors, 12(3), 3418-3437.

Mehtre, B. M. (1993). Fingerprint image analysis for automatic identification. *Machine Vision and Applications*, *6*(2), 124–139. doi:10.1007/BF01211936

Mil'shtein, S., Palma, J., Liessner, C., Baier, M., Pillai, A., & Shendye, A. (2008). Line scanner for biometric applications.Proceedings of 2008 IEEE Conference on Technologies for Homeland Security (pp. 205–208).

Milshtein, S., Pillai, A., Kunnil, V. O., Baier, M., & Bustos, P. (2011). Applications of Contactless Fingerprinting. In Tech.

Pankanti, S., Prabhakar, S., & Jain, A. (2002). On the individuality of fingerprints. *IEEE Trans. Pattern Anal.*, *24*(8), 1010–1025. doi:10.1109/TPAMI.2002.1023799

Parziale, G., Santana, E.-D., & Hauke, R. (2006). The surround imager: A multi-camera touchless device to acquire 3d rolled-equivalent fingerprints. Proceedings of*ICB, LNCS* (Vol. *3832*, pp. 244–250).

Qader, H. A., Ramli, A. R., & Al-Haddad, S. (2007). Fingerprint Recognition Using Zernike Moments. Int. Arab J. Inf. Technol., 4(4), 372-376.

Sha, L., Zhao, F., & Tang, X. (2003, September). Improved fingercode for filterbank-based fingerprint matching. *Proceedings of the 2003 International Conference on Image Processing ICIP '03* (Vol. 2, pp. 895-898). IEEE.

The Hong Kong Polytechnic University (2013). 3D Fingerprint Images Database. Retrieved from http://www.comp.polyu.edu.hk/~csajaykr/3Dfingerprint.htm

Tico, M., & Kuosmanen, P. (2003). Fingerprint matching using an orientation-based minutia descriptor. *IEEE Transactions on Pattern Analysis and Machine Intelligence*, 25(8), 1009-1014.

Virk, I.S., & Maini, R. (2012). Fingerprint image enhancement and minutiae matching in fingerprint verification. *Journal of Computing Technologies*, 2(2), 37-42.

Wang, Y., Lau, D. L., & Hassebrook, L. G. (2010). Fit-sphere unwrapping and performance analysis of 3D fingerprints. *Applied Optics*, *49*(4), 592–600. doi:10.1364/AO.49.000592 PMID:20119006

Tahirou Djara is a Postdoctoral Research Assistant at the at the Polytechnic School of Abomey-Calavi located in the University of Abomey-Calavi, Bénin. His research interests include: biometrics, signal and image processing, computational intelligence, industrial applications and symbolical programming. He is member of the research laboratory: Laboratory of Electronics, Telecommunications and Applied Data Processing Technology (Laboratoire d'Electrotechnique de Télécommunication et d'Informatique Appliquée – LETIA/EPAC). He received the Ph.D. degree in signals and image processing from the University of Abomey-Calavi, in 2013. He is a consultant in quality assurance in higher education and consultant in the field of science and engineering technology.

Marc Kokou Assogba received his PhD degree from Université Paris XII Val-de-Marne (now Université Paris-Est-Creteil UPEC) in 1999. He is Lecturer at Université d'Abomey-Calavi in Republic of Benin since 2002. prof. Assogba is very interested in Electronics, Medical Image Processing, Biometrics and Applied Computer Sciences. Prof Assogba is Director of Laboratoire d'Electrotechnique, de Télécommunication et d'Informatique Appliquée (LETIA).

Antoine Vianou is a Ph.D.-Engineer in Energy and Electricity sciences. He has been graduated through many universities as the University of Dakar and the University of Evry Val d'Essonne. He is a Full Professor in Engineering Sciences and Technologies (E.S.T.). Pr. VIANOU is currently Chairman of the Sectoral Scientific Committee of E.S.T. of the Scientific Council of UAC in Benin and is also Director of the Laboratory of Thermophysic Characterization of Materials and Energy Mastering. He is the Director of the Doctoral School of Engineering Sciences in UAC. During his academic career, Professor VIANOU taught in several African Universities and in several French ones. He is author of over hundred articles in the fields of Engineering Sciences and Technologies. In addition, he received several honors in recognition for his professional career.